Leukodystrophy resembling Vanishing White Matter Disease is recapitulated by brain-specific depletion of apoptosis regulator MCL-1

Running title: MCL-1 is required for white matter integrity

Abigail H. Cleveland[1,2], Alejandra Romero[3], Laurent Alfonso Azcona[2], Melisa Herrero[4], Viktoriya D. Nikolova[5,6], Sheryl Moy[5,6], Orna Elroy-Stein[4,7], Vivian Gama[3,8,9] and Timothy R. Gershon[2,10,11]

[1]UNC Cancer Cell Biology Training Program, University of North Carolina, Chapel Hill, North Carolina 27599, USA

[2]Department of Neurology, UNC School of Medicine, University of North Carolina, Chapel Hill, North Carolina 27599, USA

[3]Vanderbilt University, Cell and Developmental Biology, Nashville, Tennessee 37232, USA .

[4]Shmunis School of Biomedicine and Cancer Research, Faculty of Life Sciences, Tel Aviv University, Tel Aviv, Israel

[5]UNC Carolina Institute for Developmental Disabilities

[6]Department of Psychiatry, UNC School of Medicine, University of North Carolina, Chapel Hill, North Carolina 27599, USA

[7]Sagol School of Neuroscience, Tel Aviv University, Tel Aviv, Israel

[8]Vanderbilt University, Vanderbilt Center for Stem Cell Biology, Nashville, Tennessee 37232, USA .

[9]Vanderbilt University, Vanderbilt Brain Institute, Nashville, Tennessee 37232, USA .

[10]UNC Neuroscience Center, University of North Carolina, Chapel Hill, North Carolina 27599, USA

[11]Lineberger Comprehensive Cancer Center, University of North Carolina, Chapel Hill, North Carolina 27599, USA

Co-corresponding authors: Vivian Gama (vivian.gama@vanderbilt.edu) and Timothy R. Gershon (gershont@neurology.med.unc.edu)

SUMMARY

Diverse mutations cause leukodystrophies through unresolved processes. Developing leukodystrophy therapies requires identifying mechanisms that operate downstream of causative mutations to produce white matter degeneration. We have identified the apoptosis regulator MCL-1 as required for white matter stability and depleted by leukodystrophy-causing mutations. Brain-specific deletion of *Mcl-1* in mice recapitulates progressive leukodystrophy, with MRI changes, decreased oligodendrocytes, and astrocytic and microglial changes typical of Vanishing White Matter Disease (VWMD). Disabling apoptosis through co-deletion of *Bax* or *Bak* rescued white matter *Mcl-1*-dependence, broadly implicating the intrinsic apoptotic pathway in leukodystrophy pathogenesis. *Bax* and *Bak* co-deletions rescued different aspects of the *Mcl-1*-deleted phenotype, demonstrating their discrete roles in white matter stability. MCL-1 protein abundance was reduced in *eif2b5*-mutant mice that model VWMD, suggesting a mechanistic relationship between MCL-1 and VWMD. Our data show that oligodendrocytes require MCL-1 to suppress apoptosis, implicate MCL-1 loss in VWMD pathogenesis, and suggest inhibiting apoptosis for leukodystrophy therapy.

Introduction

Leukodystrophies are a heterogeneous group of severe neurodegenerative disorders marked by progressive white matter disruption (Raymond, 2017, van der Knaap and Bugiani, 2017). The age of onset varies in each leukodystrophy, but patients typically become symptomatic during childhood, after a latent, asymptomatic period (Kohler et al., 2018, Kohlschutter and Eichler, 2011). Patients with leukodystrophies may experience progressive symptoms including ataxia, dementia,

59 hallucinations, seizures, coma, and death (Vanderver et al., 1993). There is currently
60 no specific targeted therapy that has been clinically implemented to arrest the
61 progression of any leukodystrophy.

62 Diverse pathogenic mutations have been linked to different leukodystrophies
63 (van der Knaap and Bugiani, 2018), but the mechanistic processes through which
64 specific mutations cause white matter degeneration are incompletely understood.
65 Mutations in the apoptotic regulator *APOPT1* (aka *COA8*) cause Progressive
66 Cavitating Leukoencephalopathy, suggesting a role for inappropriate apoptosis in this
67 disease (Melchionda et al., 2014, Yasuda et al., 2006). However, it is not clear why
68 this mutation specifically affects cells of the white matter. Mutations in *eIF2B* subunits
69 result in Vanishing White Matter Disease (VWMD), another leukodystrophy similarly
70 marked by white matter cavitation (Bugiani et al., 2018, van der Knaap et al., 1997,
71 van der Knaap et al., 1993). The causative role of *eIF2B* mutations implicates
72 impaired mRNA translational regulation in VWMD pathogenesis, associated with
73 activation of the Integrated Stress Response (ISR) (van der Knaap et al., 2006, Fogli
74 et al., 2002, Leegwater et al., 2001, Bugiani et al., 2010, Abbink et al., 2019, Kantor
75 et al., 2005). Prior studies have not identified a role for apoptosis in VWMD causation,
76 as seen in Progressive Cavitating Leukoencephalopathy, and whether a common
77 pathogenic process unites these similar phenotypes is unclear.

78 Studies in *eIf2b5* $^{R132H/R132H}$ mice provide insight into the disproportionate effect
79 of *eIF2B* mutations on white matter. These mice develop leukodystrophy resembling
80 VWMD and show impaired mitochondrial function in fibroblasts, astrocytes, and
81 oligodendrocytes (Herrero et al., 2019, Raini et al., 2017, Geva et al., 2010). These
82 studies suggest that *eIF2B* mutations disproportionately affect white matter because
83 glia are more dependent than other types cells on accurate translational regulation

84 and mitochondrial function (Elroy-Stein, 2017). However, several unresolved steps
85 are required to connect the biological processes that have been found to be disrupted
86 in Progressive Cavitating Leukoencephalopathy and VWMD to the observed disease
87 process of progressive leukodystrophy.

88 Identifying proteins that are both required for white matter integrity and
89 affected by *eIF2B* mutations may show specific mechanisms that link VWMD
90 genotype and phenotype. Defining these mechanistic links may show why diverse
91 leukodystrophy mutations produce the final common pathology of white matter
92 degeneration. Identifying proximal mediators of white matter degeneration may also
93 provide important insight into leukodystrophy pathogenesis and treatment.

94 Here we report that mice with conditional deletion of the anti-apoptotic
95 regulator *Mcl-1* targeted to brain stem cells develop progressive postnatal white
96 matter degeneration that recapitulates the phenotype of human leukodystrophies,
97 particularly VWMD. MCL-1 promotes the survival of different cell lineages through its
98 ability to inhibit the pro-apoptotic proteins BAK and BAX, the main effectors of cell
99 death in mammalian cells. Importantly, MCL-1 is a mitochondrial protein that is
100 translationally suppressed by ISR activity (Fritsch et al., 2007), while VWMD disrupts
101 mitochondria and activates the ISR, raising the possibility the MCL-1 deficiency could
102 play a role in the VWMD phenotype.

103 *Mcl-1*-deleted mice were born with normal brain anatomy and show normal
104 motor control and behavior at postnatal day 7 (P7), but then develop increasingly
105 severe ataxia, abnormal motor responses, and extensive white matter atrophy. This
106 white matter-predominant neurodegenerative process closely matches the course of
107 human leukodystrophies with similar postnatal onset of symptoms, MRI changes,
108 progressive white matter degeneration, reduced oligodendrocyte populations,

109 astrocytic abnormalities, and microglial accumulation. Mutations that block the
110 intrinsic apoptotic pathway rescued the phenotype of *Mcl-1* deletion, implicating
111 apoptosis in leukodystrophy pathogenesis, and suggesting a potential approach to
112 therapy.

113

114

115 **Results**

116 **Conditional *Mcl-1* deletion in the CNS causes progressive white matter**
117 **degeneration.**

118 We generated mice with conditional, brain-specific *Mcl-1* deletion by breeding
119 *Mcl-1*$^{loxP/loxP}$ mice that harbor loxP sites around exon 1 of the *Mcl1* locus (Dzhagalov
120 et al., 2007), with *GFAP-Cre* mice that express Cre recombinase in stem cells that
121 give rise to the neurons and glia of the cerebrum and cerebellum, excluding the
122 Purkinje cells (Supp fig. 1A-B) (Zhuo et al., 2001, Kuang et al., 2012). The resulting
123 *hGFAP-Cre/Mcl-1*$^{loxP/loxP}$ (*Mcl-1*^{cKO}) mice were born at the expected Mendelian ratio.
124 We compared *Mcl-1*^{cKO} mice to littermate controls, including *Mcl-1*$^{loxP/loxP}$ mice without
125 Cre and heterozygously deleted *hGFAP-Cre/Mcl-1*$^{loxP/+}$. We found no differences
126 between control genotypes and therefore pooled them for analysis. In contrast, *Mcl-*
127 *1*^{cKO} mice appeared normal at P7 but developed increasing ataxia, could not be
128 weaned, and died between P20-23.

129 Examination of the brains of *Mcl-1*^{cKO} showed progressive white matter
130 degeneration, that began after the first week of life, with relative sparing of gray
131 matter. At P7, *Mcl-1*^{cKO} brains showed no abnormalities and appeared similar to

132 controls (Fig. 1A, P7). At P14, *Mcl-1*^{cKO} mice showed white matter rarefaction and
133 ventricular dilation and these changes were more pronounced at P21 (Fig. 1A,
134 P14&21). In addition to white matter loss, we also noted migration abnormalities in
135 the cerebellum, with ectopic cerebellar granule cells in the molecular layer of the
136 cerebellum (Fig. 1A). *Mcl-1*^{cKO} thus showed progressive pathology with white matter
137 loss beginning after P7 and increasing over time.

138 ***Mcl-1* deletion in the neuronal lineage does not reproduce white matter loss**

139 The *GFAP-Cre* transgenic line induces recombination in a broad lineage that
140 includes both glia and neurons (Zhuo et al., 2001). In order to determine whether *Mcl-*
141 *1* loss in neurons drives the *Mcl-1*^{cKO} phenotype, we deleted *Mcl-1* with the neuron-
142 specific *EMX1-Cre* by crossing *Mcl-1*$^{loxP/loxP}$ and *EMX1-Cre* mouse lines. The
143 resulting *EMX1-Cre/Mcl-1*$^{loxP/loxP}$ mice did not develop white matter degeneration or
144 ventriculomegaly (Fig. 1B). In contrast, deletion of *Mcl-1* in *Nestin-Cre/Mcl-1*$^{loxP/loxP}$
145 mice produced white matter degeneration as seen in *Mcl-1*^{cKO} mice (Supp Fig. 2).
146 *Nestin-Cre*, like *GFAP-Cre*, drives recombination in stem cells with neural and glial
147 potential. The preserved neuroanatomy in *EMX1-Cre/Mcl-1*$^{loxP/loxP}$ mice in contrast to
148 the ventriculomegaly and white matter degeneration in *Mcl-1*^{cKO} and *Nestin-Cre/Mcl-*
149 *1*$^{loxP/loxP}$ mice demonstrates a glial-specific dependence on MCL-1 that is not shared
150 by neurons.

151

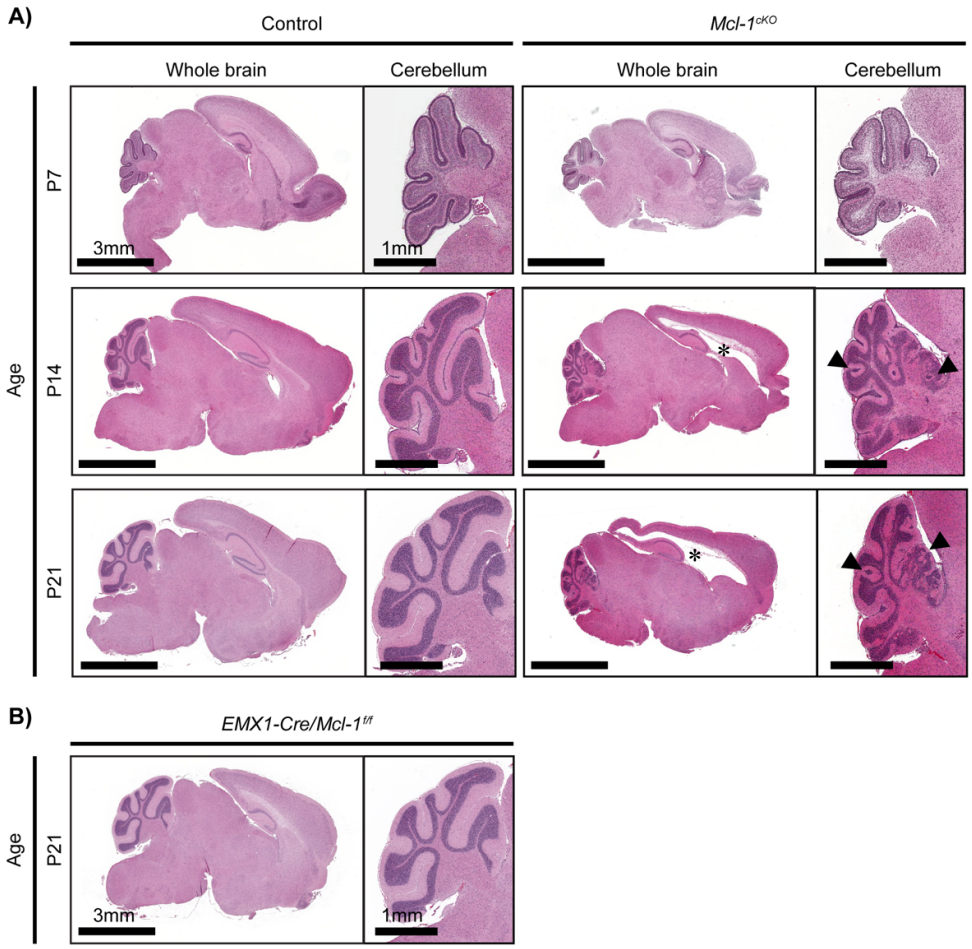

Figure 1. *Mcl-1* deletion causes progressive white matter degeneration. (**A**) Brains of representative *Mcl-1*^{cKO} mice shown in H&E-stained sagittal sections appear similar to controls at P7. By P14, *Mcl-1*^{cKO} mice develop white matter degeneration with ventricular enlargement (*) and abnormal migration of cerebellar granule neurons (arrows). White matter loss increases by P21. (**B**) Deleting *Mcl-1* in the neuron-specific *Emx* lineage in *EMX1-Cre/Mcl-1*$^{loxP/loxP}$ mice does not recapitulate the *Mcl-1*^{cKO} phenotype.

Consistent with the onset of neuropathology after P7, *Mcl-1*^{cKO} mice showed no behavioral deficits during the first week of life and gained weight similarly to controls but by P14, *Mcl-1*^{cKO} mice showed reduced weight gain (Fig. 2A) and progressive neurologic impairment. *Mcl-1*^{cKO} mice demonstrated progressive abnormalities of motor function. We used developmentally adjusted tests to compare

165 behavior of *Mcl-1*^{cKO} mice and controls at P7, P14, and P18. To examine behavior at
166 P7, when mice do not yet have open eyes and do not venture from the nest, we used
167 a test of geotaxis by placing mice on a tilted screen and measuring latency to turn.
168 We also measured latency to turn over in a righting test, and we counted pivots during
169 a 3-min open field test. We found no genotype-specific differences at P7 (Table 1).

Test	WT	*Mcl-1*^{cKO}
Negative geotaxis (latency, s)		
Trial 1	15.4 ± 2	14.3 ± 3
Trial 2	15.1 ± 2	16.7 ± 3
Trial 3	15.3 ± 2	20.9 ± 3
Righting (latency, s)	8.2 ± 1	10.0 ± 3
Number of pivots	1.7 ± 0.3	1.3 ± 0.5

170 **Table 1. Neonatal behavior testing showed no effects of *Mcl-1*^{cKO} genotype**
171 **at P7.** Each test was performed on 48 replicate WT pups and 13 replicate *Mcl-1*^{cKO}
172 pups at P7. Measures included latency to turn on a tilted screen in a test for
173 geotaxis, and latency to turn over in a righting test. Pivots were counted by an
174 experimenter during a 3-min open field test. One-way ANOVA found no statistically
175 significant differences.

176 In contrast to the similar behaviors at P7, by P14 *Mcl-1*^{cKO} mice showed
177 decreased rearing when placed in an open field and spent more time in the center of
178 the open field, while traveling similar distances compared to controls (Fig. 2B; Supp
179 fig. 1C). P18 *Mcl-1*^{cKO} mice also showed a marked increase in limb clasping when
180 vertically suspended (Fig. 2C), a commonly used marker of disease progression in a
181 number of mouse models of neurodegeneration and ataxia (Guyenet et al., 2010,
182 Nakamura et al., 2016). Responses to sensory input were also abnormal in *Mcl-1*^{cKO}
183 mice and changed over time. At P14, mice showed increased amplitude of acoustic

startle response (Fig. 2D). By P21, when motor function was significantly impaired, the amplitude of acoustic startle response was markedly diminished compared to controls. *Mcl-1*^{cKO} mice thus show reduced inhibition in response to sensory stimuli at P14, and reduced motor responses at later ages. The motor and sensory tests show progressive behavior abnormalities that correspond temporally with the white matter degeneration, beginning at P12 and worsening by P18-21.

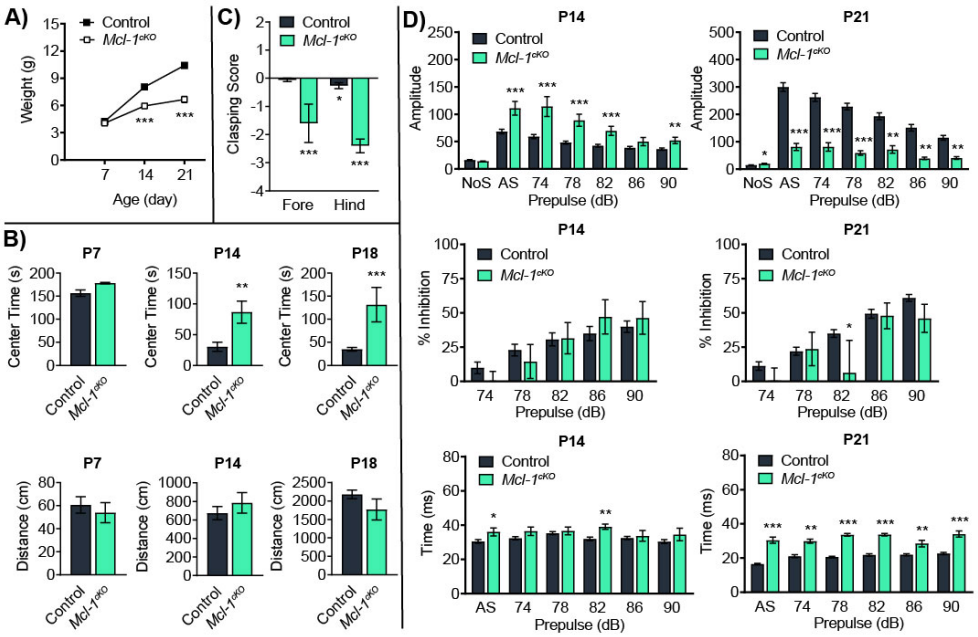

Figure 2. *Mcl-1* deletion causes progressive motor impairment and white matter degeneration. (**A**) Reduced weight gain in *Mcl-1*^{cKO} mice compared to controls. (**B**) *Mcl-1*^{cKO} mice show normal motor function at P7, with altered motor function by P14 and (**C**) increased hind-limb clasping at P18. (**D**) *Mcl-1*^{cKO} mice show increased startle in response to auditory stimuli at P14, and reduced elicited movement at P21. *, ** and *** denote $p<0.05$, $p<0.01$ and $p<0.001$ respectively, relative to controls.

Blocking apoptosis prevents white matter degeneration in *Mcl-1*-deleted mice.

To determine if white matter degeneration in *Mcl-1*^{cKO} mice resulted from increased apoptosis, we examined cell death through cleaved caspase-3 immunohistochemistry and TUNEL assays. We did not detect an increase in cleaved

201 caspase-3-stained cells at P7, prior to the onset of white matter loss, or at P14, after
202 white matter loss was evident (data not shown). However, TUNEL staining, performed
203 at P11 when white matter loss was developing, demonstrated increased cell death in
204 *Mcl-1*^{cKO} brains, consistent with a pro-apoptotic effect of *Mcl-1* deletion (Fig. 3A).

205 To determine whether the increased cell death in *Mcl-1*-deleted mice was
206 causally related to the white matter degeneration, we tested whether blocking
207 apoptosis through co-deletion of either *Bax* or *Bak* rescued the *Mcl-1*^{cKO} phenotype.
208 We repeatedly intercrossed *Mcl-1*^{cKO} mice with *Bax*$^{loxP/LoxP}$/*Bak*$^{-/-}$ mice to generate
209 animals with conditional deletion of *Mcl-1* and heterozygous or homozygous deletion
210 of *Bax* or *Bak*. We then raised pups of each genotype and analyzed survival,
211 neurologic function, and neuropathology.

212 We found that co-deletion of *Bax* or *Bak* significantly suppressed the *Mcl-1*^{cKO}
213 phenotype, but resulted in different, mitigated phenotypes. *Mcl-1*-deleted mice with
214 heterozygous co-deletion of *Bak*, with the genotype *hGFAP-Cre/Mcl1*$^{loxP/loxP}$/*Bak*$^{-/+}$
215 (*Mcl-1*^{cKO}/*Bak*$^{-/+}$), showed normal survival without overt neurologic deficits and normal
216 white matter and cerebellar migration (Fig. 3B). In contrast, *Mcl-1*-deleted mice with
217 heterozygous co-deletion of *Bax*, with the genotype *hGFAP-Cre/Mcl1*$^{loxP/loxP}$/*Bax*$^{loxP/+}$
218 (*Mcl-1*^{cKO}/*Bax*$^{fl/+}$), showed a progressive leukoencephalopathy phenotype similar *Mcl-*
219 *1*^{cKO} mice (Fig. 3B). Immunohistochemistry demonstrated markedly lower BAK
220 protein in *Bak*$^{+/-}$ animals (Fig. 3C), indicating that that heterozygous *Bak* deletion was
221 sufficient to alter BAK expression. The rescued phenotype of *Mcl-1*^{cKO}/*Bak*$^{-/+}$ mice
222 therefore demonstrated reducing BAK protein expression was sufficient to prevent
223 white matter degeneration.

224

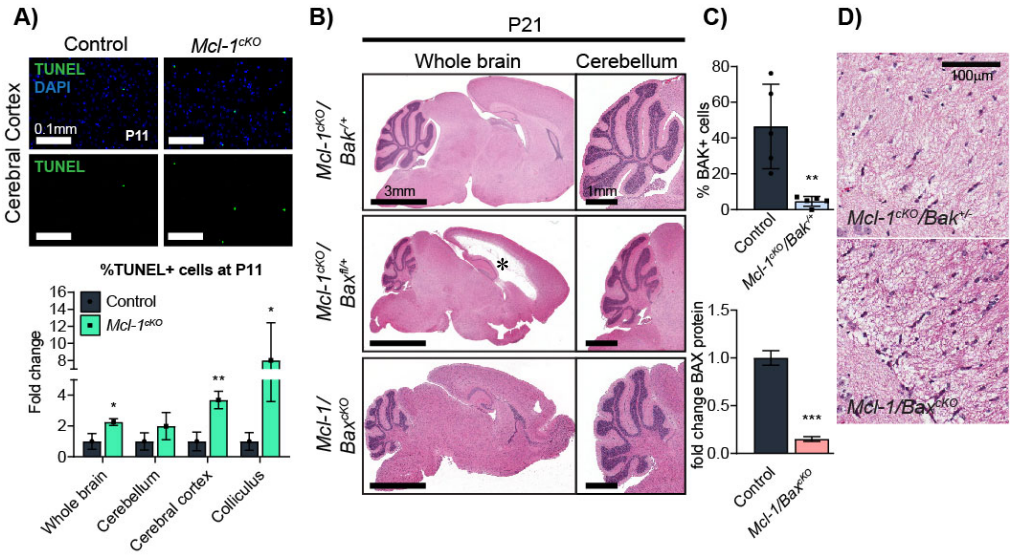

Figure 3. *Mcl-1* deletion causes white matter degeneration by increasing apoptosis. (**A**) TUNEL demonstrates increased cell death in *Mcl-1*^{cKO} brains. For cell counts, one sagittal section from each replicate was scanned at 20x and TUNEL+ cells were counted across the entire portion of each designated region that was contained within the section. (**B**) Representative H&E sections show that heterozygous *Bak* co-deletion and homozygous *Bax* co-deletion both rescue the white matter loss with ventricular enlargement (*) and cerebellar abnormalities caused by *Mcl-1* deletion. (**C**) Quantification of BAK immunohistochemistry in corpus callosum shows that heterozygous *Bak* deletion significantly reduces the number of BAK+ cells. Quantification of western blot of whole cerebella shows that homozygous *Bax* deletion reduces BAX protein abundance. (**D**) Representative images of the corpus callosum in P14 mice of the indicated genotypes shows mild white matter rarefaction in *Mcl-1/Bax*^{dKO} mice, not seen in *Mcl-1*^{cKO}*/Bak*$^{+/-}$ mice. *, ** and *** denote $p<0.05$, $p<0.01$ and $p<0.001$ respectively, relative to controls.

Mcl-1-deleted mice with homozygous *Bax* co-deletion, with the genotype *hGFAP-Cre/Mcl1*$^{loxP/loxP}$*/Bax*$^{loxP/loxP}$ (*Mcl-1/Bax*^{dKO}) showed normal survival, similar to *Mcl-1*^{cKO}*/Bak*$^{-/+}$ mice. Compared to *Mcl-1*^{cKO} mice, *Mcl-1/Bax*^{dKO} mice showed greatly reduced neurologic deficits; however, we noted that by 200 days, *Mcl-1/Bax*^{dKO} showed a slight delay in movement on opening the cage that was not seen in *Mcl-*

245 *1^{cKO}/Bak$^{+/-}$* mice. The extensive white matter loss in *Mcl-1^{cKO}* mice was rescued in
246 *Mcl-1/Bax^{dKO}* mice (Fig. 3B). Close examination of brain sections from *Mcl-1/Bax^{dKO}*
247 mice, however, showed mild white matter loss (Fig. 3D). The rescued phenotypes of
248 *Mcl-1^{cKO}/Bak$^{-/+}$* and *Mcl-1/Bax^{dKO}* mice show that disrupting either *Bax* or *Bak* is
249 sufficient to prevent the severe white matter degeneration that otherwise results from
250 *Mcl-1* deletion, implicating apoptosis in the pathogenesis of the *Mcl-1^{cKO}* phenotype.
251 The mild neurologic deficits and white matter loss in *Mcl-1/Bax^{dKO}* mice showed that
252 co-deletion of *Bax* and *Bak* do not have identical effects in *Mcl-1*-deleted animals.

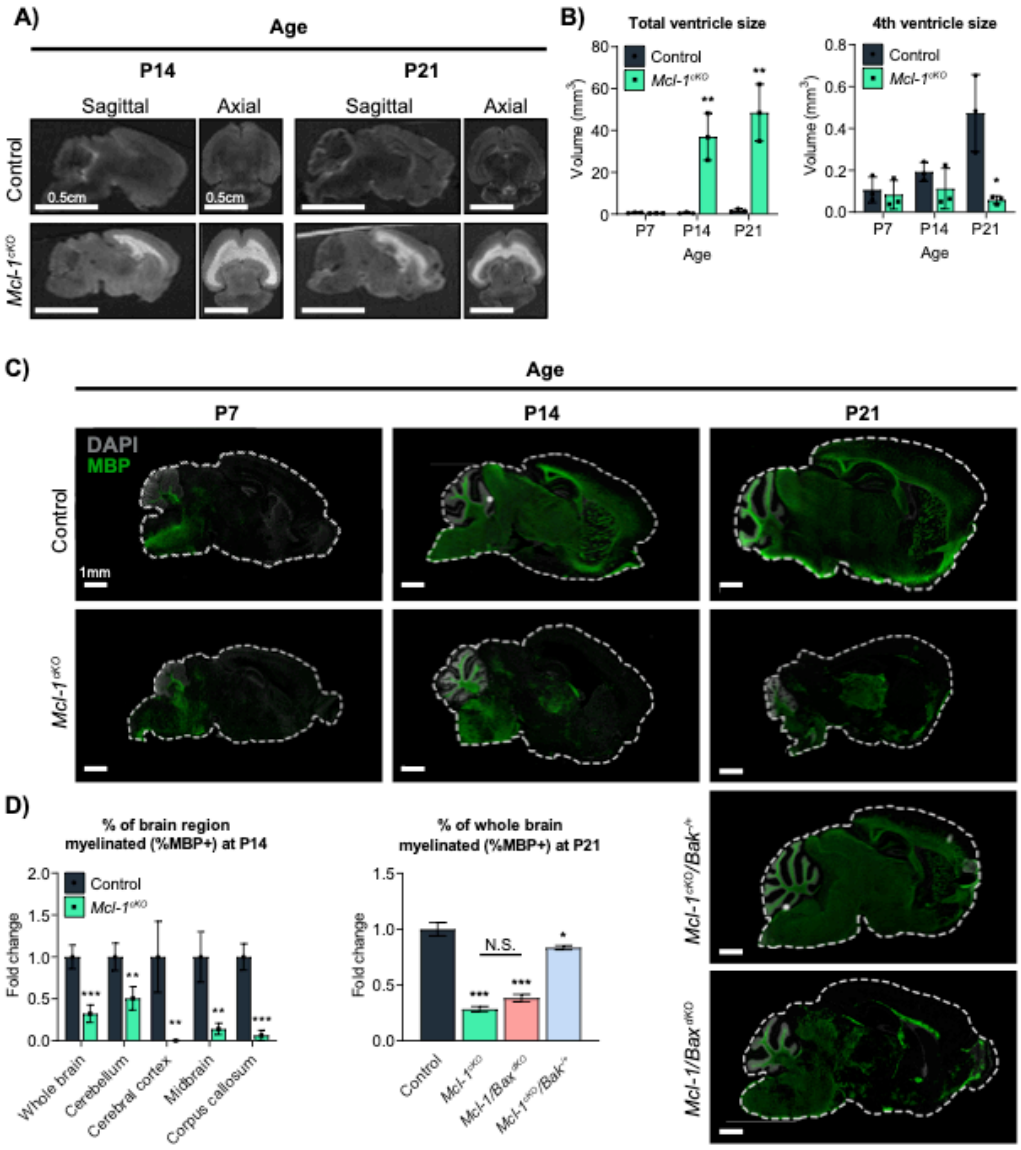

253

254 **Figure 4. Abnormal neuroimaging and myelination in *Mcl-1*-deleted mice, with**
255 **different rescue effects caused by co-deletion of *Bak* or *Bax*.** (**A**) Representative
256 MRIs show white matter hyperintensity in *Mcl-1*^{cKO} mice. (**B**) Total ventricular volume
257 is abnormal in *Mcl-1*^{cKO} mice and increases from P7-P21, while the volume of the 4th
258 ventricle decreases significantly by P21. (**C,D**) Representative images and
259 quantitative analysis of MBP IHC show that myelination is markedly decreased in *Mcl-*
260 *1*^{cKO} mice, rescued in *Mcl-1*^{cKO}*/Bak*$^{+/-}$ mice, and incompletely rescued in *Mcl-1/Bax*^{dKO}

261 mice. **(D)** Graphs show MBP+ area/total area within individual sections, normalized
262 to the mean value in the control mice. *, ** and *** denote $p<0.05$, $p<0.01$ and
263 $p<0.001$ respectively, relative to controls.

264 **Mcl-1 deletion phenocopies human leukodystrophies**

265 Leukoencephalopathies in patients produce characteristic MRI findings,
266 including high water signal in white matter tracts (Vanderver et al., 1993), and the
267 replacement of white matter by cerebrospinal fluid (van der Knaap et al., 1993). We
268 analyzed whether *Mcl-1*^{cKO} mice showed similar white matter changes on MRI. Similar
269 to VWMD patients, *Mcl-1*^{cKO} mice showed progressive ventriculomegaly (Fig. 4A).
270 The increase in ventricle size was not evenly distributed, however, as the volume of
271 the 4th ventricle was significantly smaller in *Mcl-1*^{cKO} mice at P21 (Fig. 4B). Increased
272 lateral ventricles and reduced 4th ventricle was consistent with loss of periventricular
273 cerebral white matter and an overall reduction in intracranial pressure, indicating
274 hydrocephalus *ex vacuo*.

275 To determine whether myelination was disrupted in *Mcl-1*^{cKO} mice, we
276 analyzed the distribution of Myelin Basic Protein (MBP). In control brains, the MBP+
277 area increased markedly from P7 to P14 (Fig. 4C). In contrast, myelination was
278 delayed in *Mcl-1*^{cKO} brains, which showed significantly less MBP+ area at P14 in all
279 brain regions analyzed (Fig. 4D).

280 Analysis of MBP+ area in *Mcl-1*-deleted mice with *Bax* or *Bak* co-deletions
281 showed that myelination required MCL-1 specifically to regulate BAK. We compared
282 brains in P21 animals, when normal brains show widespread myelination.
283 Heterozygous *Bak* co-deletion largely rescued myelination in *Mcl-1*^{cKO}*/Bak*$^{+/-}$ mice. In
284 these animals, MBP+ area was over 2-fold greater than in *Mcl-1*^{cKO} mice, although

285 we noted a small, statistically significant decrease in myelination compared to *Mcl-1*
286 intact controls. Homozygous *Bax* deletion, however, did not rescue myelination in
287 *Mcl-1/Bax*^{dKO} mice (Fig. 4D). The differential effects of *Bak* or *Bax* deletion on
288 myelination support the interpretation that BAX and BAK act in cells with different
289 functions, with both BAX and BAK affecting white matter maintenance, and only BAK
290 affecting myelination.

291

292 ***Mcl-1* deletion reduces oligodendrocyte and Bergmann glia populations**

293 To determine if impaired myelination in *Mcl-1*^{cKO} mice resulted from
294 oligodendrocyte loss, we compared the numbers of cells expressing the
295 oligodendrocyte marker SOX10 in *Mcl-1*^{cKO} and control mice (Fig. 5A). SOX10 marks
296 the oligodendrocyte lineage from the initial fate commitment in oligodendrocyte
297 precursors to the maturation of myelinating oligodendrocytes (Glasgow et al., 2014,
298 Nishiyama et al., 2016); SOX10 cell counts thus reflect the total oligodendrocytic
299 population across the differentiation spectrum. At P7, oligodendrocyte populations in
300 *Mcl-1*^{cKO} mice were not significantly different from controls. By P14, *Mcl-1*^{cKO} mice
301 showed significantly fewer SOX10+ cells in diverse brain regions (Fig. 5B), indicating
302 a global decrease in oligodendrocytic cells. At P21, oligodendrocytic populations
303 remained reduced in the cerebellum, corpus callosum, and superior colliculus, but
304 were not statistically significantly reduced in the hippocampus and cerebral cortex,
305 raising the possibility of a dynamic, homeostatic response in these gray matter
306 regions.

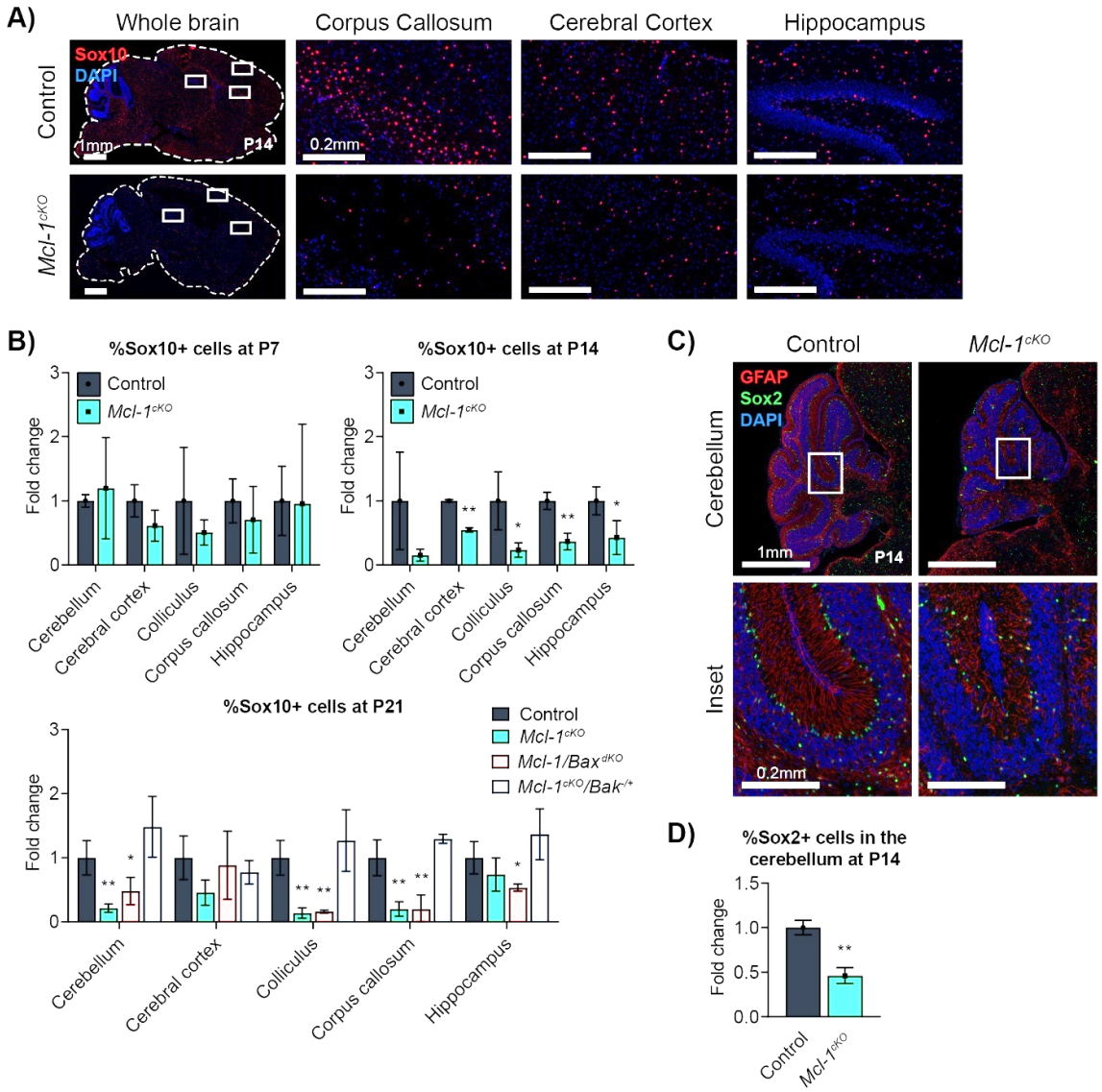

Figure 5. *Mcl-1* deletion causes loss of oligodendrocytes and Bergmann glia that is rescued with regional variation by co-deletion of *Bak* or *Bax*. (**A,B**) Representative images and quantification of SOX10 IHC in the indicated genotypes. (**C**) Representative immunofluorescence for GFAP and SOX2 IHC identify Bergmann glia in P14 mice of indicated genotypes. (**D**) SOX2+ cells are significantly reduced in *Mcl-1*^{cKO} mice. * and ** denote $p<0.05$ and $p<0.01$ respectively, relative to controls.

To determine if apoptosis mediates the decline in the oligodendrocyte populations in *Mcl-1*-deleted mice, we examined the effect of *Bax* or *Bak* co-deletion in *Mcl-1*^{cKO}*/Bak*$^{+/-}$and *Mcl-1/Bax*^{dKO} mice. Heterozygous *Bak* co-deletion in *Mcl-*

317 *1^{cKO}/Bak$^{+/-}$* mice normalized oligodendrocyte population size, but homozygous *Bax*
318 deletion in *Mcl-1/Bax^{cKO}* mice did not (Fig. 5B). *Bak* co-deletion thus rescued the
319 effects of *Mcl-1* deletion on white matter volume, myelination, and total
320 oligodendrocyte populations. In contrast, *Bax* co-deletion rescued only white matter
321 volume, but myelination and oligodendrocyte numbers remained affected in *Mcl-*
322 *1/Bax^{dKO}* mice. The discordant effects of *Bak* and *Bax* co-deletions suggest that MCL-
323 1 discretely controls BAK-dependent apoptosis or BAX-dependent apoptosis in
324 different types of white matter cells.

325 In contrast to the discordant effects of *Bax* and *Bak* co-deletions in
326 oligodendrocytes, Bergmann glia were rescued by either co-deletion. We examined
327 Bergmann glia because of their known involvement in VWMD (Dooves et al., 2016),
328 and because of the migration abnormalities in *Mcl-1^{cKO}* mice, as Bergmann glia guide
329 cerebellar granule neuron progenitors as they migrate to the internal granule cell layer
330 to become cerebellar granule neurons (Hatten, 1990, Rakic, 1971). We identified
331 Bergmann glia as cells with SOX2+ nuclei and GFAP+ processes (Fig. 5C). At P7,
332 the numbers of Bergmann glia in *Mcl-1^{cKO}* were similar to control mice (data not
333 shown), but by P14, the Bergmann glia populations in *Mcl-1^{cKO}* mice were significantly
334 reduced (Fig. 5D). The loss of Bergmann glia during the period of CGN migration
335 account for the observed cerebellar migration defects. Co-deletion of either one copy
336 of *Bak* in *Mcl-1^{cKO}/Bak$^{+/-}$* mice or both copies of *Bax* in *Mcl-1/Bax^{dKO}* mice was
337 sufficient to rescue cerebellar migration, indicating that MCL-1 functions in Bergmann
338 glia to restrict an apoptotic program that requires both BAX AND BAK in order to drive
339 cell death.

340

341

342 ***Mcl-1* deletion alters the astrocytic populations**

343 While *Mcl-1*^{cKO} mice contained fewer Bergmann glia, we noted increased
344 numbers of GFAP+ astrocytic processes throughout the brain, that was most
345 conspicuous in the relatively hypocellular molecular layer of the cerebellum (Fig. 6A).
346 To determine if this increase in GFAP+ cells indicated an increase in the total number
347 of astrocytes or an increase in the fraction of astrocytes expressing GFAP, we
348 compared the number of cells expressing the astrocytic nuclear marker SOX9 in *Mcl-*
349 *1*^{cKO} mice and controls (Fig. 6B). SOX9+ cells were not significantly increased in *Mcl-*
350 *1*^{cKO} mice in any brain region at either P7 or P14, and rather were decreased in the
351 corpus callosum at P14 (Fig. 6B,C). The increase in GFAP+ processes in *Mcl-1*^{cKO}
352 mice without the increase in SOX9+ cells shows the *Mcl-1* deletion did not increase
353 the total astrocyte population, but rather increased the fraction of astrocytes
354 expressing GFAP, indicating a reactive response to injury (Eddleston and Mucke,
355 1993, Dahl and Bignami, 1974).

356 The intermediate filament protein NESTIN is known to be up-regulated in
357 reactive astrocytes (Tamagno and Schiffer, 2006, Schmidt-Kastner et al., 2005, Sahin
358 Kaya et al., 1999, Clarke et al., 1994), and prior studies report increased Nestin-
359 expressing astrocytes in white matter from humans with VWMD (Bugiani et al., 2011).
360 Similarly, *eIF2B5* $^{R191H/R191H}$ mice show increased astrocytes expressing both Nestin
361 and GFAP in the corpus callosum, compared to wildtype controls (Dooves et al.,
362 2016, Geva et al., 2010). To determine if *Mcl1*-deleted mice also showed similar
363 astrocytic changes, we compared Nestin+/GFAP+ populations in P14 *Mcl-1*^{cKO} mice
364 and controls (Fig. 6D). *Mcl-1*^{cKO} mice demonstrated increased fractions of

365 Nestin+/GFAP+ cells in the corpus callosum (Fig 5E), with a trend toward increased
366 fractions in other white matter regions, consistent with astrocytic changes in VWMD
367 patients and *eIF2B5* $^{R191H/R191H}$ mice. *Mcl-1*^{cKO} mice thus recapitulated both the
368 astrocytic and oligodendrocytic abnormalities seen in VWMD in patients and the
369 VWMD mouse models.

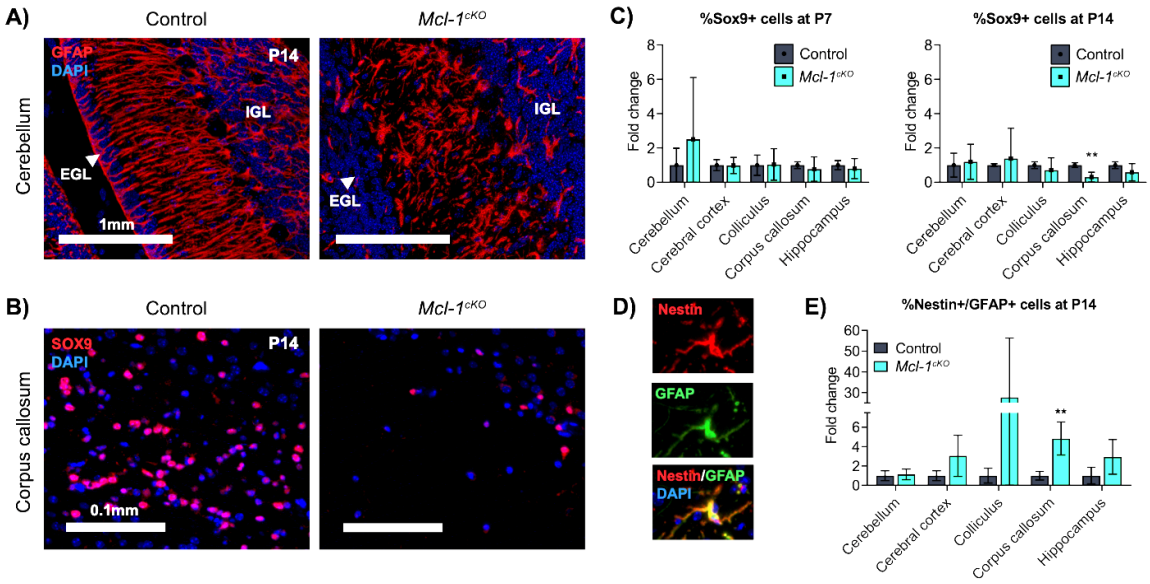

370

371 **Figure 6. Mcl-1 deletion causes reactive astrocytosis.** (**A**) Representative GFAP
372 IHC in sections of P14 cerebella in the indicated genotypes shows Bergmann glia
373 processes in the control mice that are absent in the *Mcl-1*^{cKO}, and numerous astrocyte
374 processes in the *Mcl-1*^{cKO} mice. (**B**) Representative SOX9 IHC in sections of P14
375 corpus callosum in the indicated genotypes show a significant decrease of SOX9+
376 cells in the *Mcl-1*^{cKO} mice. (**C**) Quantification of SOX9 IHC at the indicated ages and
377 genotypes, showing that astrocyte numbers are not increased in *Mcl-1*^{cKO} mice. (**D,E**)
378 Nestin/GFAP IHC, with representative images and quantification in the indicated
379 genotypes. * and ** denote $p<0.05$ and $p<0.01$ respectively, relative to controls.

380 **Mcl-1 deletion causes neuroinflammation**

381 Brains of *Mcl-1*^{cKO} mice contained increased cells expressing the myeloid
382 marker IBA1 (Fig. 7A), indicating microglial activation (Ito et al., 1998, Imai et al.,

383 1996). The microglial changes in *Mcl-1*^{cKO} mice began later than the astrocytic and
384 oligodendrocytic changes, beginning at the corpus callosum at P14; by P21, *Mcl-1*^{cKO}
385 mice showed increased IBA+ cells in diverse brain regions (Fig. 7B). The increased
386 IBA1+ microglia in *Mcl-1*^{cKO} mice demonstrates a non-cell autonomous effect in which
387 *Mcl-1* deletion in the glio-neuronally restricted GFAP lineage induced inflammatory
388 changes in myeloid cells.

389 Co-deletion of either *Bak* or *Bax* prevented microgliosis in different brain
390 regions. Heterozygous co-deletion of *Bak* in *Mcl-1*^{cKO}*; Bak*$^{+/-}$ mice significantly
391 reduced IBA1+ cells in the cerebellum, cerebral cortex, colliculus, and corpus
392 callosum, relative to *Mcl-1*^{cKO} mice. In contrast, homozygous co-deletion of *Bax* in
393 *Mcl-1*$^{/}$*Bax*^{dKO} mice showed a significant decrease in IBA1+ cells in the hippocampus,
394 relative to both *Mcl-1*^{cKO} and *Mcl-1*^{cKO}*/Bak*$^{+/-}$ mice (Fig. 7B). The rescue of neuro-
395 inflammation by co-deletion of *Bax* or *Bak* implicates increased regional apoptosis as
396 the cause of inflammation, while the region-specific pattern of rescue further supports
397 the conclusion that white matter cells in different areas of the brain alternatively
398 regulate apoptosis through interactions of MCL-1 with either BAX or BAK.

399 **Decreased brain MCL-1 protein in a VWMD mouse model**

400 Based on the similarity of the *Mcl-1*^{cKO} phenotype to VWMD, the role of the ISR in
401 VWMD, and the regulation of MCL-1 abundance by the ISR, we investigated whether
402 changes in MCL-1 protein might mediate the effect of mutant eIF2B on glial cells. To
403 begin to test this possibility, we compared MCL-1 abundance in brain lysates from
404 wildtype and *eIF2B5* $^{R132H/R132H}$ mice at 7 and 10 months old (Fig. 7C). We found that
405 by 10 months, *eIF2B5* $^{R132H/R132H}$ mice expressed reduced MCL-1 protein in the brain,
406 indicating that the *eIF2B5* $^{R132H/R132H}$ mutation results in reduced MCL-1 expression

407 over time. In *eIF2B5* $^{R132H/R132H}$ mice, the temporal course of reduced brain MCL-1
408 protein correlated with the development of VWMD symptoms. Thus, along with our
409 finding that MCL-1 deficiency in *Mcl-1*^{cKO} mice was sufficient to cause a VWMD
410 phenotype, we found declining MCL-1 expression in *eIF2B5* $^{R132H/R132H}$ mice that
411 model VWMD.

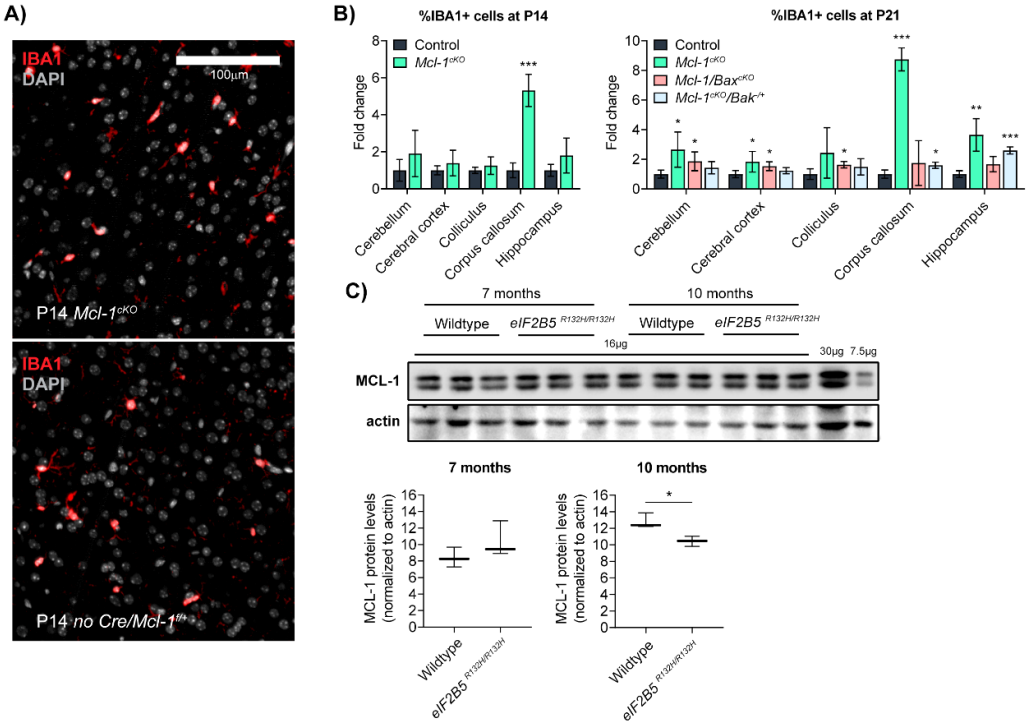

412

413 **Figure 7. Progressive neuroinflammation in *Mcl-1*^{cKO} mice and reduced MCL-1**
414 **protein in mice with VWMD.** (**A,B**) IBA1 IHC, with representative images and
415 quantification in the indicated genotypes, showing a progressive increase in microglia
416 in *Mcl-1*^{cKO} mice, beginning in the corpus callosum at P14 and expanding to include
417 diverse regions by P21. Co-deletion of *Bak* or *Bax* variably rescue microgliosis with
418 different effects in different regions. *, ** and *** denote p<0.05, p<0.01 and p<0.001
419 respectively, relative to controls. (**C**) Western blot comparing MCL-1 protein
420 abundance in brain lysates of 7- and 10-months old WT and *eIF2B5*$^{R132H/R132H}$ mice,
421 demonstrating reduced MCL-1 in 10-month old mutant mice. * denotes p<0.03,
422 relative to controls.

423 **Discussion**

424 Our data show that conditional deletion of anti-apoptotic *Mcl-1* in neuro-glial
425 stem cells results in a progressive encephalopathy with post-natal white matter
426 degeneration. While prior studies have shown increased apoptosis in embryonic and
427 adult neural progenitors resulting from *Mcl-1* deletion (Fogarty et al., 2019, Hasan et
428 al., 2013, Malone et al., 2012), our data show that brain-wide *Mcl-1* deletion produces
429 postnatal brain white matter degeneration that closely resembles the human
430 leukodystrophy VWMD. Although MCL-1 mutations have not been described in any
431 human leukodystrophy, the mechanisms of white matter injury in human
432 leukodystrophies are unresolved. Our studies show that disruption of MCL-1-
433 dependent apoptosis control in the entire brain specifically impacts white matter and
434 is sufficient to produce leukodystrophy.

435 The *Mcl-1*^{cKO} phenotype presented striking similarities to human
436 leukodystrophies, and most specifically to VWMD. Brain function and white matter
437 appeared normal in *Mcl-1*^{cKO} mice until after P7, when mice showed motor and
438 sensory impairment, delayed myelination, and rarefaction of the periventricular white
439 matter and corpus callosum, eventually leading to white matter loss and
440 hydrocephalus *ex vacuo*. Similar to VWMD, mature myelinating oligodendrocytes
441 were markedly reduced, Bergmann glia of the cerebellum were also affected, and
442 astrocytes showed reactive changes that are also seen in astrocytes in VWMD,
443 including up-regulation of GFAP and NESTIN. The similarity of the *Mcl-1*^{cKO} and
444 VWMD phenotypes, including the overall histopathology of vanishing white matter
445 and the specific loss of terminally differentiated oligodendrocytes and Bergmann glia,

446 show that *eIF2B* mutations and *Mcl-1* deletion affect specific cells of the brain in a
447 similar manner.

448 Taken together, reduced MBP and SOX10 demonstrate that within global
449 oligodendrocyte depletion of *Mcl-1*^{cKO} mice, mature, myelinating oligodendrocytes are
450 particularly affected. Studies in VWMD patients and mouse models show that while
451 mature oligodendrocyte populations are reduced, immature oligodendrocyte
452 precursors may actually be increased (Herrero et al., 2019, Bugiani et al., 2013). A
453 similar increase in immature oligodendrocytes may occur in the *Mcl-1*^{cKO} mice and
454 would not be inconsistent with the observed overall reductions in SOX10+ brain cells
455 and brain myelination.

456 The similarity of the *Mcl-1*^{cKO} phenotype to VWMD raises the possibility that
457 reduced MCL-1 protein abundance specifically contributes to VWMD pathology. The
458 known activation of the ISR in VWMD (Abbink et al., 2019, Kantor et al., 2005) and
459 the suppression of MCL-1 translation by the ISR together provide a potential
460 molecular mechanism to link the *Mcl-1*^{cKO} phenotype to VWMD. Consistent with this
461 proposed mechanism, we found reduced MCL-1 protein in *eIF2B5* $^{R132H/R132H}$ mice,
462 which correlated with the development of white matter pathology. While studies in
463 patient-derived samples could potentially test whether MCL-1 abundance is altered
464 in VWMD patients, these studies would require samples that preceded fulminant
465 white matter loss, in order to include oligodendrocyte populations that may be lost
466 through apoptosis. Our data show that MCL-1 deficiency is sufficient to reproduce the
467 VWMD phenotype in mice. Studies of *Bax* and *Bak* deletion in *eIF2B5* $^{R132H/R132H}$ mice
468 would allow testing of whether apoptosis is required for VWMD.

469 The rescue of the *Mcl-1*^{cKO} phenotype by co-deletion of *Bak* or *Bax* implicate
470 apoptosis in the causation of white matter loss in *Mcl-1*^{cKO} mice. We previously found
471 that conditional *Mcl-1* deletion in cerebellar granule neuron progenitors does not
472 produce a phenotype of gray matter loss as these cells regulate BAX via the
473 homologous anti-apoptotic protein BCL-xL *(Crowther et al., 2013)*. The specific
474 dependencies of different cell types on different anti-apoptotic factors is also seen
475 outside the nervous system, as in the myeloid lineage where neutrophils undergo
476 spontaneous apoptosis when *Mcl-1* is deleted, but macrophages survive (Dzhagalov
477 et al., 2007). Different cell types within broad lineages may thus require different anti-
478 apoptotic family proteins to regulate apoptosis, and the survival of neurons and
479 astrocytes in *Mcl-1*^{cKO} mice shows that within the broad lineage derived from glio-
480 neuronal stem cells, MCL-1 protein is specifically required by a subset of cells at some
481 point along the more narrow lineage of the oligodendrocytes.

482 In addition to demonstrating the requirement for apoptosis in white matter
483 degeneration in *Mcl-1*^{cKO} mice, the *Bax* and *Bak* rescue studies demonstrate that
484 myelination defects and white matter loss can be dissociated. Co-deletion of *Bak*
485 rescued both myelination, oligodendrocyte populations, and white matter loss. In
486 contrast co-deletion of *Bax* reduced white matter loss without rescuing myelination
487 and oligodendrocyte populations. These differences show that different cell types that
488 can be differentiated by their apoptosis regulation contribute to different aspects of
489 the *Mcl-1*^{cKO} phenotype.

490 The possibility that BAX and BAK act in different cells with different sensitivities
491 does not require differential expression patterns. For example, prior studies show that
492 both BAX and BAK can drive apoptosis in cerebellar granule neuron progenitors, but

493 under different conditions. BAX-dependent apoptosis in these cells can be engaged
494 either by radiation-induced DNA damage (Chong et al., 2000), or by chromosomal
495 fragmentation in the setting of *Atr* deletion (Lang et al., 2016). In contrast, BAK-
496 dependent apoptosis is not engaged by radiation, as radiation induced apoptosis is
497 blocked by *Bax* deletion(Crowther et al., 2013, Chong et al., 2000); BAK-dependent
498 apoptosis requires the more intense trigger of *Atr* deletion and resulting chromosomal
499 fragmentation (Lang et al., 2016). These prior studies show that cells in the CNS that
500 express both BAX and BAK can show different mechanisms and sensitivities for
501 triggering BAX-dependent or BAK-dependent apoptosis. Similarly, specific subsets of
502 glia may regulate BAX-dependent and BAK-dependent apoptosis through different
503 mechanisms, with different, cell-type specific sensitivities and dependencies on MCL-
504 1.

505 The rescue myelination by co-deletion of *Bak* but not *Bax* shows that
506 myelinating oligodendrocytes or their precursors regulate apoptosis specifically
507 through MCL-1:BAK interactions. The different rescue pattern with *Bax* co-deletion,
508 which prevented white matter degeneration without normalizing myelination, shows
509 that a different type of cell regulates white matter loss and requires both BAK and
510 BAX to be present for *Mcl-1* deletion to produce phenotype changes. Clearly, diverse
511 cell types are affected in both *Mcl-1*^{cKO} mice and VWMD patients (Bugiani et al., 2018,
512 Zhou et al., 2019). Our genetic rescue studies show that different types of glial cells
513 depend on MCL-1 to regulate different pro-apoptotic proteins, and that loss of this
514 regulation in different types of cells reproduces different aspects of the overall
515 pathology. The loss of multiple subsets of glial cells may similarly contribute to
516 different aspects of the overall VWMD phenotype.

While multiple mutations can cause leukodystrophies, for many of these genetic diseases, the mechanistic steps from mutation to white matter loss remain to be specified in detail. Our findings that MCL-1 deletion in neuro-glial stem cells produces white matter degeneration, and that this degeneration is rescued by co-deletion of *Bax* or *Bak* implicates the process of apoptosis in the causation of leukodystrophy. Moreover, our rescue experiments show that apoptosis in multiple cell types derived from neuro-glial stem cells contribute to different aspects of white matter pathology. Treatments that inhibit the intrinsic apoptotic pathway in the postnatal brain may provide an avenue for reducing the impact of diverse leukodystrophies.

Acknowledgments: supported by R01NS088219 (TRG), R01NS102627 (TRG), and R01NS1062 (TRG), T32CA071341 (AHC), 4R00CA178190 (VG), R35GM128915 (VG), and R21CA227483 (VG), U54 HD079124 (VDM,SM).

Author Contributions: Conceptualization, T.R.G. and V.G.; Methodology, A.H.C., V.D.M., S.M, T.R.G., V.G. and O.E-S.; Investigation, A.H.C, V.D.M., A.R., L.A.A., M.H.,; Writing – Original Draft, A.H.C. and T.R.G.; Writing – Review & Editing, O.E-S., S.M., V.G. and T.R.G; Funding Acquisition, V.G., and T.R.G.;; Resources, O.E-S., V.G., and T.R.G.; Supervision, S.M.,O.E-S., V.G., and T.R.G.

Methods

Mice

We generated *Mcl-1*^{cKO} mice, by crossing *GFAP-Cre* mice (Jackson Labs, stock # 004600) with *Mcl-1*$^{LoxP/LoxP}$ mice (Dzhagalov et al., 2007), generously shared by Dr. You-Wen He. We interbred GFAP-Cre, *Mcl-1*$^{loxP/loxP}$, and *Bax*$^{LoxP/LoxP}$*/Bak*$^{-/-}$ (Jackson Labs, stock # 006329) to generate *Mcl-1;Bax*^{dKO}, *Mcl-1;Bak*^{dKO}, and various

544 heterozygous controls. We generated *EMX1-Cre/Mcl-1*$^{loxP/loxP}$ mice by breeding
545 *EMX1-Cre* mice, generously provided by Dr. William Snide, into the *Mcl-1 f/f* line. All
546 mice were of species *Mus musculus* and crossed into the C57BL/6 background
547 through at least five generations. All animal studies were carried out with the approval
548 of the University of North Carolina Institutional Animal Care and Use Committee
549 under protocols (19-099).

550 Wild type (C57BL/6 strain) and *eIF2B5*$^{R132H/R132H}$ mice (Geva et al., 2010) were
551 generated, bred, and housed in Tel Aviv University animal facility (Lab Products Inc.,
552 Seaford, DE, USA). All experimental procedures were approved by the Tel Aviv
553 University Animal Care Committee according to national guidelines (permit #04-17-
554 022). Breeding and genotyping were performed as previously described. (Geva et al.,
555 2010) Each generation was established by back cross of homozygous
556 *eIF2B5*$^{R132H/R132H}$ mice with WT C57BL/6J (Harlan Labs, Jerusalem, Israel) to prevent
557 genetic drift.

558

559 **Histology and immunohistochemistry (IHC)**

560 Mouse brains were processed and immunostained as previously described (Ocasio
561 et al., 2019, Tech et al., 2017, Lang et al., 2016, Crowther et al., 2016). Primary
562 antibodies used were: BAK diluted 1:200 (Cell Signaling, #12105), MBP diluted
563 1:1000 (Abcam, #ab7349), SOX10 diluted 1:100 (Santa Cruz, #sc-17342), cleaved-
564 Caspase 3 (cC3) diluted 1:400 (Biocare Medical, #CP229C), glial fibrillary acidic
565 protein (GFAP) diluted 1:2000 (Dako, Z0334), SOX2 1:200 (Cell Signaling, #4900S),
566 SOX9 1:200 (R&D Systems, #AF3075), NESTIN 1:500 (Cell Signaling, #4760), IBA1
567 1:2000 (Wako Chemicals, #019-19741). Stained images were counterstained with

568 DAPI, digitally imaged using an Aperio Scan Scope XT (Aperio) and subjected to
569 automated cell counting using Tissue Studio (Definiens).
570
571 **Magnetic resonance imaging**
572 For MRI studies, brains from P7, P14, and P21 mice were harvested and fixed in 4%
573 formaldehyde in PBS for 48hrs, then transferred to PBS. Brains were then embedded
574 in 2% agarose in 15mL plastic vials and imaged in pairs as previously described
575 (Williams et al., 2015).
576
577 **Western blot**
578 Whole brains or cerebella were harvested and homogenized in lysis buffer (Cell
579 Signaling, #9803). Lysate protein concentrations were quantified using a
580 bicinchoninic acid (BCA) protein assay kit (Thermo scientific, #23225). Equal total
581 protein concentrations were resolved on SDS-polyacrylamide gels (BioRad, #
582 4561105, # 4568094) and transferred onto polyvinylidene difluoride membranes.
583 Membranes were blotted using a SNAP i.d. 2.0 Protein Detection System (Millipore).
584 Membranes were imaged using a chemiluminescent SuperSignal West Femto
585 Maximum Sensitivity Substrate (34095, Thermo Fisher Scientific) and the C-DiGit blot
586 scanner (LI-COR Biosciences). Signal was quantified using the Image Studio Lite
587 software (LI-COR). The following antibodies were used for western blot: MCL-1 (Cell
588 Signaling, #94296; 1:500 dilution), BAX (Cell Signaling, #14796; 1:500 dilution), β-
589 actin (Cell Signaling, #3700; 1:5000 dilution), Actin (Sigma #A3853; 1:240000
590 dilution), Anti-rabbit IgG, HRP-linked antibody (Cell Signaling, #7074; 1.5:1000
591 dilution), Anti-mouse IgG, HRP-linked antibody (Cell Signaling, #7076; 1.5:1000
592 dilution). For the eIF2B5$^{R132H/R132H}$ studies, cerebrums were harvested from 7 and 10

593 month old mice and protein was extracted using a lysis buffer containing 1% triton,
594 0.5% NaDOC, 0.1% SDS, 50 mM Tris pH 8, 100 mM NaCl, 10 mM β-
595 glycerophosphate, 5 mM NaF, 1 mM DTT, 1 mM vanadate, and EDTA-free complete
596 TM protease inhibitor cocktail (#11-836-170-001; ROCHE). Protein was quantified
597 using a BCA protein assay kit (#23227 Pierce), diluted in 1X sample buffer (0.05 M
598 HEPES pH 7.4, 2% (w/v) SDS, 10% (v/v) Glycerol, traces of Bromophenol Blue, 100
599 mM Dithiothreitol (DTT)), and separated on a 10% SDS-PAGE gel. Blots were imaged
600 using an AI600 Imager (Amersham) and quantified by ImageQuant TL (GE
601 Healthcare, Pittsburgh, PA, United States).
602
603 **Behavioral studies**
604 **Animals included.** Subjects were *Mcl-1*^{cKO} mice or littermate controls with intact Mcl-
605 1, including genotypes Mcl1$^{f/+}$ without Cre, Mcl1$^{f/f}$ without Cre, and Gfap-Cre/Mcl1$^{f/+}$.
606 A total of 8 litters were needed to generate all of the replicates. Day of birth was
607 considered postnatal day 0 (P0). Subject numbers at the beginning of the study (P7)
608 were 13 (21%) *Mcl-1*^{cKO} and 48 (79%) control. All litters completed the first 2 weeks
609 of testing. Three litters (n=23) were removed from the study for histology assays
610 during the third week of testing: one on P15, after the second open field test; one on
611 PD16, after the first acoustic startle test; and one on P21, after the tail suspension
612 test.
613
614 **Behavioral testing regimen**
615 **Developmentally-calibrated behavioral tests:** For motor tests at P7, mice were
616 removed from the home cage and maintained in a beaker warmed to 35°C. Mice were

617 then subjected to the neurobehavioral negative geotaxis, righting, and open field
618 tests, adapted from published studies (Cheh et al., 2006).
619 **Negative geotaxis**. A 20 cm × 20 cm screen with 0.5 cm wire mesh squares was set
620 at a 25° angle. Each pup was placed downward on the screen with its head facing
621 toward the bottom, allowed to grip the mesh, and then released. The time it took for
622 each pup to turn 180° (head and upper torso vertical), was recorded, with a 30 s
623 maximum and each pup was tested 3 times.
624 **Righting.** Each pup was placed onto its back on a flat Plexiglas surface. The
625 experimenter gently held the pup in place for 2 s and then released it. The latency to
626 righting (all 4 feet on the ground) was timed, with a maximum of 30 s.
627 **Open field activity and pivoting.** Each pup was placed into the center of a Plexiglas
628 chamber (PhenoTyper; 30.5 cm × 30.5 cm × 43.5 cm; Noldus Information
629 Technology, Wageningen, The Netherlands). A dim yellow light (30 lx) at the top of
630 the PhenoTyper box was illuminated throughout the 3 min trial. Measures were taken
631 of distance traveled and time in the center region (4 cm × 4 cm square in the center
632 of the arena) by an image-tracking system (EthoVision, Noldus Information
633 Technology). In addition, the experimenter recorded the number of vertical rearing
634 movements and number of pivots (circling or lateral movement, as opposed to
635 forward locomotion).
636 Each mouse was screened through the 3 assays in the order presented here. After
637 finishing the neonatal motor screen, each pup was weighed, marked with a non-toxic
638 Sharpie, and placed back into the warm beaker. The litter was returned to the home
639 cage after all pups had been tested.
640

641 **Open field activity at P14 and P19.** Additional open field activity tests were
642 performed at P14 and P19. The distance traveled, the number of vertical rearing
643 movements, and time spent in the center region was recorded in each 10 min test.
644
645 **Acoustic startle responses.** This test was used to assess auditory function,
646 reactivity to environmental stimuli, and sensorimotor gating. Mice were evaluated at
647 2 time points, P14 and P21. The procedure was based on the reflexive whole-body
648 flinch, or startle response, that follows exposure to the acoustic stimuli. Measures
649 were taken of startle magnitude and prepulse inhibition, which occurs when a weak
650 stimulus leads to a reduced startle in response to a subsequent louder noise.
651 Mice were placed into individual Plexiglas cylinders within larger, sound-
652 attenuating chambers. Each cylinder was seated upon a piezoelectric transducer,
653 which allowed vibrations to be quantified and displayed on a computer (San Diego
654 Instruments SR-Lab system). The chambers included a ceiling light, fan, and a
655 loudspeaker for the acoustic stimuli. Background sound levels (70 dB) and calibration
656 of the acoustic stimuli were confirmed with a digital sound level meter (San Diego
657 Instruments). Each session began with a 5-min habituation period, followed by 42
658 trials of 7 different types: no-stimulus (NoS) trials, trials with the acoustic startle
659 stimulus (AS; 40 msec, 120 dB) alone, and trials in which a prepulse stimulus (20
660 msec; either 74, 78, 82, 86, or 90 dB) occurred 100 ms before the onset of the startle
661 stimulus. Measures were taken of the startle amplitude for each trial across a 65-
662 msec sampling window, and an overall analysis was performed for each subject's
663 data for levels of prepulse inhibition at each prepulse sound level (calculated as 100
664 - [(response amplitude for prepulse stimulus and startle stimulus together / response
665 amplitude for startle stimulus alone) x 100].

666

667 **Limb clasping.** At PD18-21, a subset of mice (n=39) was assessed for limb clasping
668 during a tail-suspension test. Each mouse was lifted by the base of the tail, and
669 suspended above cage bedding for 15 sec, with ventral (stomach) side facing the
670 experimenter. Response to tail suspension was coded using the following scoring
671 system:

672

673 Forepaw movement
674 -2 = paws are clasped together, little movement, may be drawn up against
675 chest
676 0 = paws move quickly in periodic flailing or kicking motions
677 2 = vigorous movement, may resemble rapid digging
678 Hindlimb placement and movement
679 -4 = both hindlimbs are retracted inwards toward abdomen, with little
680 movement
681 -2 = hindlimbs are partially or intermittently retracted inwards toward abdomen
682 0 = hindlimbs are splayed outward from the abdomen. Moderate kicking behavior
683 2 = vigorous rapid kicking

684

685 **Statistical analysis of behavioral tests**

686 All testing was conducted by experimenters blinded to mouse genotype. Statview
687 (SAS, Cary, NC) was used for data analyses. To reduce the number of *Mcl-1*^{cKO}
688 subjects required, behavioral data from males and females were combined. One-
689 way or repeated measures analysis of variance (ANOVA) were used to determine
690 effects of genotype. Post-hoc analyses were conducted using Fisher's Protected

691 Least Significant Difference (PLSD) tests following a significant ANOVA F value. For

692 all comparisons, significance was set at $p<0.05$.

693

694

695 **Supplementary Figures**

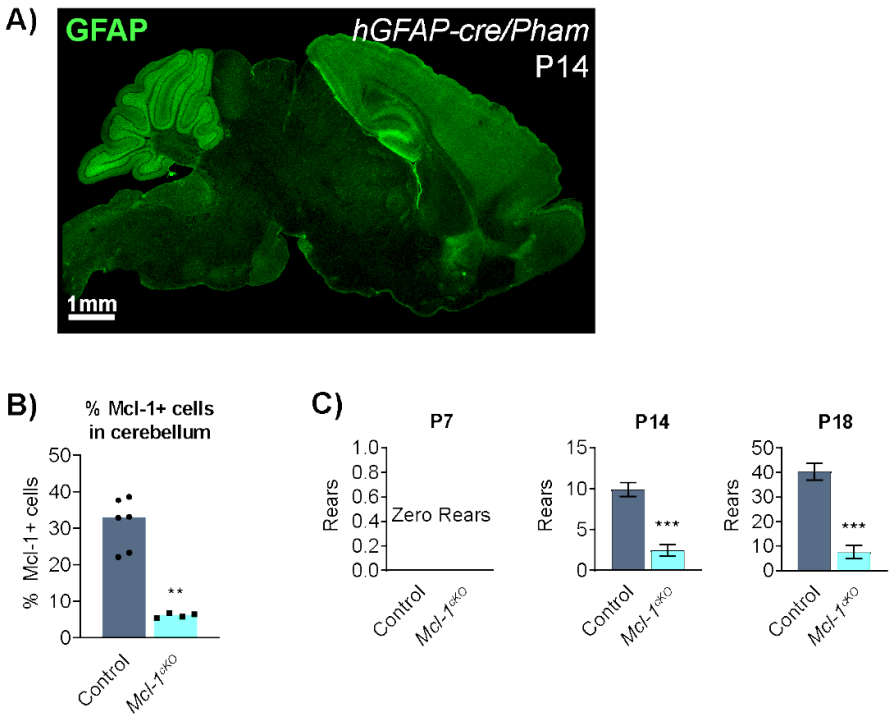

696

697 **Supplementary Figure 1. *hGFAP-Cre* conditionally deletes *Mcl-1* in regions**
698 **throughout the brain. A)** *hGFAP-Cre* induces expression of the fluorescent reporter
699 DENDRA2 in *hGFAP-cre/Pham* mice, indicating regions of GFAP expression. *hGFAP-*
700 *Cre* targets cells in diverse regions throughout the brain, including the cerebellum,
701 hippocampus, and cortex. **B)** MCL-1 protein levels are significantly reduced in
702 cerebella of *Mcl-1*^{cKO} mice. **C)** *Mcl-1*^{cKO} mice displayed decreased rearing at both P14
703 and P18.

704

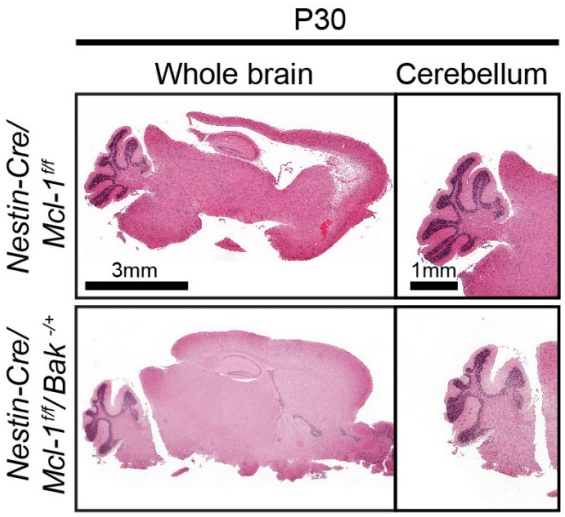

705

706 **Supplementary Figure 2. *Nestin-Cre/Mcl-1$^{f/f}$* mice develop white matter**
707 **degeneration similar to that of *Mcl-1^{cKO}* mice.** Similar to GFAP-Cre, Nestin-Cre
708 targets cells of both the neural and glial lineage. Brains harvested from *Nestin-*
709 *Cre/Mcl-1$^{f/f}$* mice showed ventricular dilation and white matter rarefaction by P30.
710 Deletion of one copy of *Bak* rescued this phenotype in *Nestin-Cre/Mcl-1$^{f/f}$/Bak$^{-/+}$* mice.

711

712

713 **References**

714 ABBINK, T. E. M., WISSE, L. E., JAKU, E., THIECKE, M. J., VOLTOLINI-GONZALEZ, D., FRITSEN,
715 H., BOBELDIJK, S., TER BRAAK, T. J., POLDER, E., POSTMA, N. L., BUGIANI, M.,
716 STRUIJS, E. A., VERHEIJEN, M., STRAAT, N., VAN DER SLUIS, S., THOMAS, A. A. M.,
717 MOLENAAR, D. & VAN DER KNAAP, M. S. 2019. Vanishing white matter: deregulated
718 integrated stress response as therapy target. *Ann Clin Transl Neurol,* 6**,** 1407-1422.
719 BUGIANI, M., BOOR, I., POWERS, J. M., SCHEPER, G. C. & VAN DER KNAAP, M. S. 2010.
720 Leukoencephalopathy with vanishing white matter: a review. *J Neuropathol Exp*
721 *Neurol,* 69**,** 987-96.
722 BUGIANI, M., BOOR, I., VAN KOLLENBURG, B., POSTMA, N., POLDER, E., VAN BERKEL, C.,
723 VAN KESTEREN, R. E., WINDREM, M. S., HOL, E. M., SCHEPER, G. C., GOLDMAN, S. A.
724 & VAN DER KNAAP, M. S. 2011. Defective glial maturation in vanishing white matter
725 disease. *J Neuropathol Exp Neurol,* 70**,** 69-82.
726 BUGIANI, M., POSTMA, N., POLDER, E., DIELEMAN, N., SCHEFFER, P. G., SIM, F. J., VAN DER
727 KNAAP, M. S. & BOOR, I. 2013. Hyaluronan accumulation and arrested
728 oligodendrocyte progenitor maturation in vanishing white matter disease. *Brain,*
729 136**,** 209-22.
730 BUGIANI, M., VUONG, C., BREUR, M. & VAN DER KNAAP, M. S. 2018. Vanishing white
731 matter: a leukodystrophy due to astrocytic dysfunction. *Brain Pathol,* 28**,** 408-421.
732 CHEH, M. A., MILLONIG, J. H., ROSELLI, L. M., MING, X., JACOBSEN, E., KAMDAR, S. &
733 WAGNER, G. C. 2006. En2 knockout mice display neurobehavioral and neurochemical
734 alterations relevant to autism spectrum disorder. *Brain Res,* 1116**,** 166-76.
735 CHONG, M. J., MURRAY, M. R., GOSINK, E. C., RUSSELL, H. R. C., SRINIVASAN, A., KAPSETAKI,
736 M., KORSMEYER, S. J. & MCKINNON, P. J. 2000. Atm and Bax cooperate in ionizing
737 radiation-induced apoptosis in the central nervous system. *Proceedings of the*
738 *National Academy of Sciences,* 97**,** 889-894.
739 CLARKE, S. R., SHETTY, A. K., BRADLEY, J. L. & TURNER, D. A. 1994. Reactive astrocytes
740 express the embryonic intermediate neurofilament nestin. *Neuroreport,* 5**,** 1885-8.
741 CROWTHER, A. J., GAMA, V., BEVILACQUA, A., CHANG, S. X., YUAN, H., DESHMUKH, M. &
742 GERSHON, T. R. 2013. Tonic activation of Bax primes neural progenitors for rapid
743 apoptosis through a mechanism preserved in medulloblastoma. *The Journal of*
744 *neuroscience : the official journal of the Society for Neuroscience,* 33**,** 18098-108.
745 CROWTHER, A. J., OCASIO, J. K., FANG, F., MEIDINGER, J., WU, J., DEAL, A. M., CHANG, S. X.,
746 YUAN, H., SCHMID, R., DAVIS, I. & GERSHON, T. R. 2016. Radiation Sensitivity in a
747 Preclinical Mouse Model of Medulloblastoma Relies on the Function of the Intrinsic
748 Apoptotic Pathway. *Cancer Res,* 76**,** 3211-23.
749 DAHL, D. & BIGNAMI, A. 1974. Heterogeneity of the glial fibrillary acidic protein in gliosed
750 human brains. *J Neurol Sci,* 23**,** 551-63.
751 DOOVES, S., BUGIANI, M., POSTMA, N. L., POLDER, E., LAND, N., HORAN, S. T., VAN DEIJK, A.
752 L., VAN DE KREEKE, A., JACOBS, G., VUONG, C., KLOOSTER, J., KAMERMANS, M.,
753 WORTEL, J., LOOS, M., WISSE, L. E., SCHEPER, G. C., ABBINK, T. E., HEINE, V. M. &
754 VAN DER KNAAP, M. S. 2016. Astrocytes are central in the pathomechanisms of
755 vanishing white matter. *J Clin Invest,* 126**,** 1512-24.
756 DZHAGALOV, I., ST JOHN, A. & HE, Y. W. 2007. The antiapoptotic protein Mcl-1 is essential
757 for the survival of neutrophils but not macrophages. *Blood,* 109**,** 1620-6.

758 EDDLESTON, M. & MUCKE, L. 1993. Molecular profile of reactive astrocytes--implications for
759 their role in neurologic disease. *Neuroscience,* 54**,** 15-36.
760 ELROY-STEIN, O. 2017. Mitochondrial malfunction in vanishing white matter disease: a
761 disease of the cytosolic translation machinery. *Neural Regen Res,* 12**,** 1610-1612.
762 FOGARTY, L. C., FLEMMER, R. T., GEIZER, B. A., LICURSI, M., KARUNANITHY, A., OPFERMAN,
763 J. T., HIRASAWA, K. & VANDERLUIT, J. L. 2019. Mcl-1 and Bcl-xL are essential for
764 survival of the developing nervous system. *Cell Death Differ,* 26**,** 1501-1515.
765 FOGLI, A., WONG, K., EYMARD-PIERRE, E., WENGER, J., BOUFFARD, J. P., GOLDIN, E., BLACK,
766 D. N., BOESPFLUG-TANGUY, O. & SCHIFFMANN, R. 2002. Cree leukoencephalopathy
767 and CACH/VWM disease are allelic at the EIF2B5 locus. *Ann Neurol,* 52**,** 506-10.
768 FRITSCH, R. M., SCHNEIDER, G., SAUR, D., SCHEIBEL, M. & SCHMID, R. M. 2007. Translational
769 repression of MCL-1 couples stress-induced eIF2 alpha phosphorylation to
770 mitochondrial apoptosis initiation. *J Biol Chem,* 282**,** 22551-62.
771 GEVA, M., CABILLY, Y., ASSAF, Y., MINDROUL, N., MAROM, L., RAINI, G., PINCHASI, D. &
772 ELROY-STEIN, O. 2010. A mouse model for eukaryotic translation initiation factor 2B-
773 leucodystrophy reveals abnormal development of brain white matter. *Brain,* 133**,**
774 2448-61.
775 GLASGOW, S. M., ZHU, W., STOLT, C. C., HUANG, T. W., CHEN, F., LOTURCO, J. J., NEUL, J. L.,
776 WEGNER, M., MOHILA, C. & DENEEN, B. 2014. Mutual antagonism between Sox10
777 and NFIA regulates diversification of glial lineages and glioma subtypes. *Nat*
778 *Neurosci,* 17**,** 1322-9.
779 GUYENET, S. J., FURRER, S. A., DAMIAN, V. M., BAUGHAN, T. D., LA SPADA, A. R. & GARDEN,
780 G. A. 2010. A simple composite phenotype scoring system for evaluating mouse
781 models of cerebellar ataxia. *J Vis Exp*.
782 HASAN, S. M., SHEEN, A. D., POWER, A. M., LANGEVIN, L. M., XIONG, J., FURLONG, M., DAY,
783 K., SCHUURMANS, C., OPFERMAN, J. T. & VANDERLUIT, J. L. 2013. Mcl1 regulates the
784 terminal mitosis of neural precursor cells in the mammalian brain through p27Kip1.
785 *Development,* 140**,** 3118-27.
786 HATTEN, M. E. 1990. Riding the glial monorail: a common mechanism for glial-guided
787 neuronal migration in different regions of the developing mammalian brain. *Trends*
788 *Neurosci,* 13**,** 179-84.
789 HERRERO, M., MANDELBOUM, S. & ELROY-STEIN, O. 2019. eIF2B Mutations Cause
790 Mitochondrial Malfunction in Oligodendrocytes. *Neuromolecular Med,* 21**,** 303-313.
791 IMAI, Y., IBATA, I., ITO, D., OHSAWA, K. & KOHSAKA, S. 1996. A novel gene iba1 in the major
792 histocompatibility complex class III region encoding an EF hand protein expressed in
793 a monocytic lineage. *Biochem Biophys Res Commun,* 224**,** 855-62.
794 ITO, D., IMAI, Y., OHSAWA, K., NAKAJIMA, K., FUKUUCHI, Y. & KOHSAKA, S. 1998. Microglia-
795 specific localisation of a novel calcium binding protein, Iba1. *Brain Res Mol Brain Res,*
796 57**,** 1-9.
797 KANTOR, L., HARDING, H. P., RON, D., SCHIFFMANN, R., KANESKI, C. R., KIMBALL, S. R. &
798 ELROY-STEIN, O. 2005. Heightened stress response in primary fibroblasts expressing
799 mutant eIF2B genes from CACH/VWM leukodystrophy patients. *Hum Genet,* 118**,** 99-
800 106.
801 KOHLER, W., CURIEL, J. & VANDERVER, A. 2018. Adulthood leukodystrophies. *Nat Rev*
802 *Neurol,* 14**,** 94-105.
803 KOHLSCHUTTER, A. & EICHLER, F. 2011. Childhood leukodystrophies: a clinical perspective.
804 *Expert Rev Neurother,* 11**,** 1485-96.

805 KUANG, Y., LIU, Q., SHU, X., ZHANG, C., HUANG, N., LI, J., JIANG, M. & LI, H. 2012. Dicer1 and
806 MiR-9 are required for proper Notch1 signaling and the Bergmann glial phenotype in
807 the developing mouse cerebellum. *Glia,* 60**,** 1734-46.
808 LANG, P. Y., NANJANGUD, G. J., SOKOLSKY-PAPKOV, M., SHAW, C., HWANG, D., PARKER, J.
809 S., KABANOV, A. V. & GERSHON, T. R. 2016. ATR maintains chromosomal integrity
810 during postnatal cerebellar neurogenesis and is required for medulloblastoma
811 formation. *Development,* 143**,** 4038-4052.
812 LEEGWATER, P. A., VERMEULEN, G., KONST, A. A., NAIDU, S., MULDERS, J., VISSER, A.,
813 KERSBERGEN, P., MOBACH, D., FONDS, D., VAN BERKEL, C. G., LEMMERS, R. J.,
814 FRANTS, R. R., OUDEJANS, C. B., SCHUTGENS, R. B., PRONK, J. C. & VAN DER KNAAP,
815 M. S. 2001. Subunits of the translation initiation factor eIF2B are mutant in
816 leukoencephalopathy with vanishing white matter. *Nat Genet,* 29**,** 383-8.
817 MALONE, C. D., HASAN, S. M., ROOME, R. B., XIONG, J., FURLONG, M., OPFERMAN, J. T. &
818 VANDERLUIT, J. L. 2012. Mcl-1 regulates the survival of adult neural precursor cells.
819 *Mol Cell Neurosci,* 49**,** 439-47.
820 MELCHIONDA, L., HAACK, T. B., HARDY, S., ABBINK, T. E., FERNANDEZ-VIZARRA, E.,
821 LAMANTEA, E., MARCHET, S., MORANDI, L., MOGGIO, M., CARROZZO, R., TORRACO,
822 A., DIODATO, D., STROM, T. M., MEITINGER, T., TEKTURK, P., YAPICI, Z., AL-
823 MURSHEDI, F., STEVENS, R., RODENBURG, R. J., LAMPERTI, C., ARDISSONE, A.,
824 MORONI, I., UZIEL, G., PROKISCH, H., TAYLOR, R. W., BERTINI, E., VAN DER KNAAP,
825 M. S., GHEZZI, D. & ZEVIANI, M. 2014. Mutations in APOPT1, encoding a
826 mitochondrial protein, cause cavitating leukoencephalopathy with cytochrome c
827 oxidase deficiency. *Am J Hum Genet,* 95**,** 315-25.
828 NAKAMURA, A., SWAHARI, V., PLESTANT, C., SMITH, I., MCCOY, E., SMITH, S., MOY, S. S.,
829 ANTON, E. S. & DESHMUKH, M. 2016. Bcl-xL Is Essential for the Survival and Function
830 of Differentiated Neurons in the Cortex That Control Complex Behaviors. *J Neurosci,*
831 36**,** 5448-61.
832 NISHIYAMA, A., BOSHANS, L., GONCALVES, C. M., WEGRZYN, J. & PATEL, K. D. 2016. Lineage,
833 fate, and fate potential of NG2-glia. *Brain Res,* 1638**,** 116-128.
834 OCASIO, J. K., BATES, R. D. P., RAPP, C. D. & GERSHON, T. R. 2019. GSK-3 modulates SHH-
835 driven proliferation in postnatal cerebellar neurogenesis and medulloblastoma.
836 *Development,* 146.
837 RAINI, G., SHARET, R., HERRERO, M., ATZMON, A., SHENOY, A., GEIGER, T. & ELROY-STEIN,
838 O. 2017. Mutant eIF2B leads to impaired mitochondrial oxidative phosphorylation in
839 vanishing white matter disease. *J Neurochem,* 141**,** 694-707.
840 RAKIC, P. 1971. Neuron-glia relationship during granule cell migration in developing
841 cerebellar cortex. A Golgi and electronmicroscopic study in Macacus Rhesus. *J Comp*
842 *Neurol,* 141**,** 283-312.
843 RAYMOND, G. V. 2017. Leukodystrophy: Basic and Clinical. *Adv Neurobiol,* 15**,** 365-382.
844 SAHIN KAYA, S., MAHMOOD, A., LI, Y., YAVUZ, E. & CHOPP, M. 1999. Expression of nestin
845 after traumatic brain injury in rat brain. *Brain Res,* 840**,** 153-7.
846 SCHMIDT-KASTNER, R., AGUIRRE-CHEN, C., SAUL, I., YICK, L., HAMASAKI, D., BUSTO, R. &
847 GINSBERG, M. D. 2005. Astrocytes react to oligemia in the forebrain induced by
848 chronic bilateral common carotid artery occlusion in rats. *Brain Res,* 1052**,** 28-39.
849 TAMAGNO, I. & SCHIFFER, D. 2006. Nestin expression in reactive astrocytes of human
850 pathology. *J Neurooncol,* 80**,** 227-33.

851 TECH, K., TIKUNOV, A. P., FAROOQ, H., MORRISSY, A. S., MEIDINGER, J., FISH, T., GREEN, S.
852 C., LIU, H., LI, Y., MUNGALL, A. J., MOORE, R. A., MA, Y., JONES, S. J. M., MARRA, M.
853 A., VANDER HEIDEN, M. G., TAYLOR, M. D., MACDONALD, J. M. & GERSHON, T. R.
854 2017. Pyruvate Kinase Inhibits Proliferation during Postnatal Cerebellar
855 Neurogenesis and Suppresses Medulloblastoma Formation. *Cancer Res,* 77**,** 3217-
856 3230.
857 VAN DER KNAAP, M. S., BARTH, P. G., GABREELS, F. J., FRANZONI, E., BEGEER, J. H., STROINK,
858 H., ROTTEVEEL, J. J. & VALK, J. 1997. A new leukoencephalopathy with vanishing
859 white matter. *Neurology,* 48**,** 845-55.
860 VAN DER KNAAP, M. S. & BUGIANI, M. 2017. Leukodystrophies: a proposed classification
861 system based on pathological changes and pathogenetic mechanisms. *Acta*
862 *Neuropathol,* 134**,** 351-382.
863 VAN DER KNAAP, M. S. & BUGIANI, M. 2018. Leukodystrophies - much more than just
864 diseases of myelin. *Nat Rev Neurol,* 14**,** 747-748.
865 VAN DER KNAAP, M. S., FOGLI, A., BOESPFLUG-TANGUY, O., ABBINK, T. E. M. &
866 SCHIFFMANN, R. 1993. Childhood Ataxia with Central Nervous System
867 Hypomyelination / Vanishing White Matter. *In:* ADAM, M. P., ARDINGER, H. H.,
868 PAGON, R. A., WALLACE, S. E., BEAN, L. J. H., STEPHENS, K. & AMEMIYA, A. (eds.)
869 *GeneReviews((R)).* Seattle (WA).
870 VAN DER KNAAP, M. S., PRONK, J. C. & SCHEPER, G. C. 2006. Vanishing white matter disease.
871 *Lancet Neurol,* 5**,** 413-23.
872 VANDERVER, A., TONDUTI, D., SCHIFFMANN, R., SCHMIDT, J. & VAN DER KNAAP, M. S. 1993.
873 Leukodystrophy Overview - ARCHIVED CHAPTER, FOR HISTORICAL REFERENCE ONLY.
874 *In:* ADAM, M. P., ARDINGER, H. H., PAGON, R. A., WALLACE, S. E., BEAN, L. J. H.,
875 STEPHENS, K. & AMEMIYA, A. (eds.) *GeneReviews((R)).* Seattle (WA).
876 YASUDA, O., FUKUO, K., SUN, X., NISHITANI, M., YOTSUI, T., HIGUCHI, M., SUZUKI, T.,
877 RAKUGI, H., SMITHIES, O., MAEDA, N. & OGIHARA, T. 2006. Apop-1, a novel protein
878 inducing cyclophilin D-dependent but Bax/Bak-related channel-independent
879 apoptosis. *J Biol Chem,* 281**,** 23899-907.
880 ZHOU, L., LI, P., CHEN, N., DAI, L. F., GAO, K., LIU, Y. N., SHEN, L., WANG, J. M., JIANG, Y. W.
881 & WU, Y. 2019. Modeling vanishing white matter disease with patient-derived
882 induced pluripotent stem cells reveals astrocytic dysfunction. *CNS Neurosci Ther,* 25**,**
883 759-771.
884 ZHUO, L., THEIS, M., ALVAREZ-MAYA, I., BRENNER, M., WILLECKE, K. & MESSING, A. 2001.
885 hGFAP-cre transgenic mice for manipulation of glial and neuronal function in vivo.
886 *genesis,* 31**,** 85-94.
887

888

889

890

891